Symmetry conditions of a nodal superconductor for generating robust flat-band Andreev bound states at its dirty surface

Satoshi Ikegaya,[1] Shingo Kobayashi,[2,3] and Yasuhiro Asano[1,4,5]

[1]*Department of Applied Physics, Hokkaido University, Sapporo 060-8628, Japan*
[2]*Department of Applied Physics, Nagoya University, Nagoya 464-8603, Japan*
[3]*Institute for Advanced Research, Nagoya University, Nagoya 464-8601, Japan*
[4]*Center of Topological Science and Technology, Hokkaido University, Sapporo 060-8628, Japan*
[5]*Moscow Institute of Physics and Technology, 141700 Dolgoprudny, Russia*

We discuss the symmetry property of a nodal superconductor that hosts robust flat-band zero-energy states at its surface under potential disorder. Such robust zero-energy states are known to induce the anomalous proximity effect in a dirty normal metal attached to a superconductor. A recent study has shown that a topological index $\mathcal{N}_{\text{ZES}}$ describes the number of zero-energy states at the dirty surface of a p-wave superconductor. We generalize the theory to clarify the conditions required for a superconductor that enables $\mathcal{N}_{\text{ZES}} \neq 0$. Our results show that $\mathcal{N}_{\text{ZES}} \neq 0$ is realized in a topological material that belongs to either the BDI or CII class. We also present two realistic Hamiltonians that result in $\mathcal{N}_{\text{ZES}} \neq 0$.

I. INTRODUCTION

In the past decade, topologically nontrivial superconductors have attracted enormous attention due to the existence of exotic bound states at their surfaces [1–3]. Early studies on this topic focused mainly on the topological phase of a fully gapped superconductor listed in the tenfold topological classification [4]. The bulk-boundary correspondence suggests the equivalence between the number of surface bound states and the absolute value of a topological invariant $\mathcal{Z}$ defined in the bulk states [5]. A unique physical consequence of such a topological superconductor might be the zero-bias conductance quantization at $G_{\text{NS}} = (2e^2/h)|\mathcal{Z}|$ in a normal-metal/superconductor (NS) junction. In experiments, however, it is not easy to observe conductance quantization clearly for the following reasons. The invariant $\mathcal{Z}$ is usually limited to small numbers in real fully gapped superconductors, whereas the number of propagating channels N_c is much larger than unity in two- or three-dimensional NS junctions. Therefore, the electric current passing through normal propagating channels would smear the effects of resonant transmission through the topological bound states.

Today, superconductors characterized by such unconventional pairing symmetry as spin-singlet d-wave and spin-triplet p-wave are considered to be topologically nontrivial, although their gap functions have nodes on the Fermi surface [6–26]. The most striking feature of such a nodal superconductor is that it hosts flat-band zero-energy states (ZESs) at its clean surface. It has been well established that the conductance of an NS junction consisting of such an unconventional superconductor is quantized at $G_{\text{NS}} = (2e^2/h)\mathcal{N}_{\text{clean}}$ [6,7,20,27–29]. Here $\mathcal{N}_{\text{clean}}$ is the number of surface bound states at zero energy and is of the order of N_c. In addition to zero-bias conductance quantization, the fractional Josephson effect [30–34], the paramagnetic response at a surface [35–40], and the anomalies

in heat transport [41] are physical phenomena unique to a nodal superconductor. Since $\mathcal{N}_{\text{clean}}$ is the same order as N_c, the effects of the surface bound states on the electromagnetic phenomena in a nodal superconductor can be more noticeable than those in a fully gapped topological superconductor. However, these statements are true as long as the surface or the junction interface of the superconductor is sufficiently clean. In experiments, potential disorder is inevitable at the surface of a superconductor and may lift the degeneracy of the flat-band bound states at zero energy. Actually, the flat-band ZESs at a surface of the d-wave superconductor are fragile under potential disorder [42,43]. On the other hand, the flat-band ZESs of the p-wave superconductor are robust [27,33]. The question is how to distinguish these two types of nodal superconductors.

A key theoretical method with which to solve the problem is called dimensional reduction, and it is a useful theoretical tool for characterizing a nodal superconductor topologically. In a d-dimensional nodal superconductor, we can still find a fully gapped one-dimensional partial Brillouin zone by fixing the $(d-1)$-dimensional momentum at a certain point (say, k). In such a one-dimensional Brillouin zone, it is possible to define a winding number $w(k)$ in terms of the wave function of the occupied states below the gap [8,9]. A nonzero winding number $w(k)$ suggests $|w(k)|$-fold-degenerate ZESs at the surface for each k. Therefore, $\mathcal{N}_{\text{clean}} = \sum_k |w(k)|$ describes the number of ZESs at the clean surface of a nodal superconductor. In contrast to the topological invariant of a fully gapped topological superconductor, $\mathcal{N}_{\text{clean}}$ cannot predict the number of ZESs at a dirty surface [44]. With the dimensional reduction, translational symmetry is necessary to define the winding number in a one-dimensional Brillouin zone. However, such partial Brillouin zones themselves are not well defined at all because the momentum k is no longer a good quantum number under potential disorder. Nevertheless, two of the

present authors have shown that an alternative index, $\mathcal{N}_{\text{ZES}} = \sum_k w(k)$, describes the number of ZESs at a dirty surface [45]. In other words, $\mathcal{N}_{\text{ZES}}$ represents the bulk-boundary correspondence of a nodal superconductor in the dirty case. Moreover, a nodal superconductor with $\mathcal{N}_{\text{ZES}} \neq 0$ is known to induce the anomalous proximity effect in dirty proximity structures such as conductance quantization at $G_{\text{NS}} = (2e^2/h)|\mathcal{N}_{\text{ZES}}|$ in a dirty NS junction [27], the fractional Josephson effect in a dirty Josephson junction [33], and the paramagnetic Meissner response at a dirty surface of a superconductor [39]. To our knowledge, $\mathcal{N}_{\text{ZES}}$ becomes nonzero in several nodal superconductors characterized by spin-triplet p- and f-wave pairing symmetries. Namely, spin-triplet p- and f-wave superconductivity is a sufficient condition for $\mathcal{N}_{\text{ZES}} \neq 0$. However, we do not know any necessary conditions for $\mathcal{N}_{\text{ZES}} \neq 0$. Such conditions would provide us with a design guide for topologically nontrivial artificial superconductors, which may be realized by applying the fabrication technique to existing materials. This paper will clarify the necessary conditions for $\mathcal{N}_{\text{ZES}} \neq 0$.

In this paper, we first study the relationship between the symmetry class of the Bogoliubov–de Gennes (BdG) Hamiltonian and the possibility of a nonzero index $\mathcal{N}_{\text{ZES}}$. Within the tenfold topological classification, the classes BDI, CII, DIII, and CI are the target symmetry classes of this paper because a nodal superconductor belonging to these symmetry classes is able to host flat-band ZESs at their clean surfaces. We find that $\mathcal{N}_{\text{ZES}} = 0$ identically in classes DIII and CI, whereas $\mathcal{N}_{\text{ZES}} \neq 0$ is realized in classes BDI and CII. The results are summarized in Table I. On the basis of this conclusion, we also seek practical examples of the BdG Hamiltonian in class BDI. As a result, we find two realistic models which describe a Dresselhaus [110] superconductor [19,20] and a helical p-wave superconductor with an in-plane magnetic field [21,22]. Thus, we conclude that these superconductors host $|\mathcal{N}_{\text{ZES}}|$-fold-degenerate ZESs at their dirty surfaces.

This paper is organized as follows. In Sec. II, we discuss the possible symmetry class of a nodal superconductor that possesses the nonzero index $\mathcal{N}_{\text{ZES}}$. On the basis of the general conclusion in Sec. II, we present realistic models of a nodal superconductor in class BDI in Sec. III. We summarize this paper in Sec. IV.

TABLE I. Relationship between the symmetry class of a nodal superconductor and the number of flat-band zero-energy states (ZESs) at its surface. The first column lists the relevant symmetry classes of the nodal superconductor. The second and third columns indicate the sign of $\mathcal{T}^2$ and $\mathcal{C}^2$, respectively. The fourth column indicates the presence of chiral symmetry by $\mathcal{S}^2 = +1$. The fifth column represents the number of flat-band ZESs at a clean surface of a nodal superconductor $\mathcal{N}_{\text{clean}} = \sum_{\boldsymbol{k}_\parallel}' |w(\boldsymbol{k}_\parallel)|$. The sixth column denotes the number of the ZESs at a dirty surface of a nodal superconductor evaluated by the index $\mathcal{N}_{\text{ZES}} = \sum_{\boldsymbol{k}_\parallel}' w(\boldsymbol{k}_\parallel)$.

	TRS	PHS	CS	Clean	Dirty
BDI	$+1$	$+1$	$+1$	$\mathcal{N}_{\text{clean}}$	$|\mathcal{N}_{\text{ZES}}|$
CII	-1	-1	$+1$	$\mathcal{N}_{\text{clean}}$	$|\mathcal{N}_{\text{ZES}}|$
DIII	-1	$+1$	$+1$	$\mathcal{N}_{\text{clean}}$	0
CI	$+1$	-1	$+1$	$\mathcal{N}_{\text{clean}}$	0

II. SYMMETRY CLASS AND TOPOLOGICAL INDEX

A. Preliminary

First, we briefly review the topological property of a time-reversal-invariant nodal superconductor. The BdG Hamiltonian in momentum space is generally given by

$$\mathcal{H}(\boldsymbol{k}) = \begin{bmatrix} h(\boldsymbol{k}) & \Delta(\boldsymbol{k}) \\ -\Delta^*(-\boldsymbol{k}) & -h^*(-\boldsymbol{k}) \end{bmatrix}, \qquad (1)$$

where $h(\boldsymbol{k})$ denotes the $N \times N$ normal-state Hamiltonian of an electron, $\Delta(\boldsymbol{k})$ is the $N \times N$ pair potential, and N represents the number of degrees of freedom such as spins and conduction bands. Time-reversal symmetry (TRS) and particle-hole symmetry (PHS) of $\mathcal{H}(\boldsymbol{k})$ are represented by

$$\mathcal{T} \mathcal{H}(\boldsymbol{k}) \mathcal{T}^{-1} = \mathcal{H}(-\boldsymbol{k}), \quad \mathcal{T} = \mathcal{U}_\mathcal{T}\mathcal{K}, \quad \mathcal{T}^2 = \pm 1, \quad (2)$$

$$\mathcal{C} \mathcal{H}(\boldsymbol{k}) \mathcal{C}^{-1} = -\mathcal{H}(-\boldsymbol{k}), \quad \mathcal{C} = \mathcal{U}_\mathcal{C}\mathcal{K}, \quad \mathcal{C}^2 = \pm 1, \quad (3)$$

where $\mathcal{U}_\mathcal{T}$ and $\mathcal{U}_\mathcal{C}$ are $2N \times 2N$ unitary operators and $\mathcal{K}$ is the complex-conjugation operator. In terms of the signs of $\mathcal{T}^2$ and $\mathcal{C}^2$, we can classify the present BdG Hamiltonian into four symmetry classes: BDI, CII, DIII, and CI [4]. The values of $(\mathcal{T}^2, \mathcal{C}^2)$ in these classes are summarized in Table I.

When a BdG Hamiltonian belongs to one of these symmetry classes, it is possible to define chiral symmetry (CS) of the Hamiltonian by

$$\mathcal{S} \mathcal{H}(\boldsymbol{k}) \mathcal{S}^{-1} = -\mathcal{H}(\boldsymbol{k}), \quad \mathcal{S} = e^{i\alpha}\mathcal{T}\mathcal{C}, \qquad (4)$$

where $\mathcal{S}$ is a unitary operator and α is an arbitrary real number. The commutation relation $[\mathcal{S}^2, \mathcal{H}(\boldsymbol{k})] = 0$ holds for any Hamiltonians preserving chiral symmetry. As a result, $\mathcal{S}^2$ is proportional to the identity operator as $\mathcal{S}^2 = e^{i\beta}$. Phase β can be removed by choosing α in an appropriate way. Thus, in the following, we assume $\mathcal{S}^2 = +1$ without loss of generality.

In the superconductor under consideration, the pair potential has nodes on the Fermi surface. Therefore, it is impossible to define a topological invariant by using the wave functions of the entire Brillouin zone. In a three- (two-) dimensional case, we assume that the pair potential has line (point) nodes on the Fermi surface. The nodal point $\boldsymbol{k}_0$ satisfies $\det[\mathcal{H}(\boldsymbol{k}_0)] = 0$. Even in the presence of the nodes, it is still possible to define a one-dimensional partial Brillouin zone by fixing the $(d-1)$-dimensional momentum $\boldsymbol{k}_\parallel$ at a certain point. When the pair potential in such a partial Brillouin zone is fully gapped, we can define the one-dimensional winding number as

$$w(\boldsymbol{k}_\parallel) = \frac{i}{4\pi} \int dk_\perp \text{Tr}[\mathcal{S}\mathcal{H}^{-1}(\boldsymbol{k})\partial_{k_\perp}\mathcal{H}(\boldsymbol{k})], \qquad (5)$$

where $k_\perp$ is the momentum in a one-dimensional Brillouin zone. The winding number $w(\boldsymbol{k}_\parallel)$ cannot be defined when the integral path along $k_\perp$ in Eq. (5) intersects the gap nodes $\boldsymbol{k}_0$.

When $w(\boldsymbol{k}_\parallel)$ is nonzero at $\boldsymbol{k}_\parallel$, according to the bulk-boundary correspondence, $|w(\boldsymbol{k}_\parallel)|$-fold-degenerate ZESs are expected at a clean surface parallel to $\boldsymbol{k}_\parallel$. Thus, the total number of ZESs at a clean surface is given by

$$\mathcal{N}_{\text{clean}} = \sum_{\boldsymbol{k}_\parallel}' |w(\boldsymbol{k}_\parallel)|, \qquad (6)$$

where $\sum_{\boldsymbol{k}_\parallel}{}'$ denotes a summation over $\boldsymbol{k}_\parallel$ excluding the nodal points. Such highly degenerate surface bound states are called flat-band ZESs because the energy dispersion is independent of $\boldsymbol{k}_\parallel$.

Next, we focus on flat-band ZESs at the dirty surface of a nodal superconductor. The surface is located at $x_\perp = 0$, and the nodal superconductor occupies $x_\perp \geqslant 0$. The potential disorder in the bulk region strongly suppresses unconventional superconductivity. Thus, we assume that the potential disorders exist only near the surface $x_\perp \ll \xi_S$, where ξ_S represents the superconducting coherence length. The nonmagnetic random potential $V(\boldsymbol{r})$ preserves TRS and PHS as

$$\mathcal{T} \, V(\boldsymbol{r}) \, \mathcal{T}^{-1} = V(\boldsymbol{r}), \tag{7}$$

$$\mathcal{C} \, V(\boldsymbol{r}) \, \mathcal{C}^{-1} = -V(\boldsymbol{r}), \tag{8}$$

where $V(\boldsymbol{r})$ is finite only for $x_\perp \ll \xi_S$. In the presence of potential disorders, the winding number $w(\boldsymbol{k}_\parallel)$ is not well defined because the momentum $\boldsymbol{k}_\parallel$ is no longer a good quantum number in the absence of translational symmetry. This implies that $w(\boldsymbol{k}_\parallel)$ cannot straightforwardly predict the number of the ZESs at a dirty surface. Nevertheless, it is possible to characterize the flat-band ZESs at a dirty surface by using an alternative index [45],

$$\mathcal{N}_{\mathrm{ZES}} = \sum_{\boldsymbol{k}_\parallel}{}' w(\boldsymbol{k}_\parallel). \tag{9}$$

The absolute value of the index $\mathcal{N}_{\mathrm{ZES}}$ coincides with the number of ZESs at the dirty surface of a nodal superconductor.

When we introduce the potential disorders in the bulk region, the potential disorders must be sufficiently weak to keep unconventional superconductivity. On the other hand, in the case of the surface disorder, the index $\mathcal{N}_{\mathrm{ZES}}$ describes the number of ZESs irrespective of its strength (see also Sec. II in Ref. [45]). In what follows, we study the relationship between the symmetry class of the Hamiltonian and the realization of the nonzero index $\mathcal{N}_{\mathrm{ZES}}$.

B. Realization of nonzero topological index

As shown in Appendix A, the commutation relations for the symmetry operators depend on the symmetry class of the Hamiltonian as follows:

$$[\mathcal{S}, \mathcal{T}] = [\mathcal{S}, \mathcal{C}] = 0 \tag{10}$$

for BDI and CII and

$$\{\mathcal{S}, \mathcal{T}\} = \{\mathcal{S}, \mathcal{T}\} = 0 \tag{11}$$

for DIII and CI. From these commutation relations, we obtain

$$\mathcal{T}^{-1} \, \mathcal{S} \, \mathcal{T} = \mathcal{U}_\mathcal{T} \, \mathcal{S}^* \, \mathcal{U}_\mathcal{T}^\dagger = \eta \, \mathcal{S}, \tag{12}$$

$$\mathcal{C}^{-1} \, \mathcal{S} \, \mathcal{C} = \mathcal{U}_\mathcal{C} \, \mathcal{S}^* \, \mathcal{U}_\mathcal{C}^\dagger = \eta \, \mathcal{S}, \tag{13}$$

$$\eta = \begin{cases} +1 & \text{for BDI and CII} \\ -1 & \text{for DIII and CI}. \end{cases} \tag{14}$$

By taking into account Eqs. (12) and (13), the complex conjugation of the winding number [46] is calculated as follows:

$$\begin{aligned}
\{w(\boldsymbol{k}_\parallel)\}^* &= -\frac{i}{4\pi} \int dk_\perp \mathrm{Tr}[\mathcal{S}^* \{\mathcal{H}^{-1}(\boldsymbol{k})\}^* \partial_{k_\perp} \mathcal{H}^*(\boldsymbol{k})] \\
&= -\frac{i}{4\pi} \int dk_\perp \mathrm{Tr}[\mathcal{S}^* \{\mathcal{U}_\Lambda^\dagger \, \mathcal{H}^{-1}(-\boldsymbol{k}) \, \mathcal{U}_\Lambda\} \, \partial_{k_\perp} \{\mathcal{U}_\Lambda^\dagger \, \mathcal{H}(-\boldsymbol{k}) \, \mathcal{U}_\Lambda\}] \\
&= -\frac{i}{4\pi} \int dk_\perp \mathrm{Tr}[\{\mathcal{U}_\Lambda \, \mathcal{S}^* \, \mathcal{U}_\Lambda^\dagger\} \mathcal{H}^{-1}(-\boldsymbol{k}) \, \partial_{k_\perp} \mathcal{H}(-\boldsymbol{k})] \\
&= \frac{i}{4\pi} \int dk_\perp \mathrm{Tr}[(\eta \mathcal{S}) \mathcal{H}^{-1}(k_\perp, -\boldsymbol{k}_\parallel) \, \partial_{k_\perp} \mathcal{H}(k_\perp, -\boldsymbol{k}_\parallel)] \\
&= \eta \, w(-\boldsymbol{k}_\parallel),
\end{aligned} \tag{15}$$

where $\Lambda = \mathcal{T}$ or $\mathcal{C}$. In the second line of Eq. (15), we use the relations

$$\mathcal{H}^*(\boldsymbol{k}) = \mathcal{U}_\mathcal{T}^\dagger \, \mathcal{H}(-\boldsymbol{k}) \, \mathcal{U}_\mathcal{T}, \tag{16}$$

$$\mathcal{H}^*(\boldsymbol{k}) = -\mathcal{U}_\mathcal{C}^\dagger \, \mathcal{H}(-\boldsymbol{k}) \, \mathcal{U}_\mathcal{C}, \tag{17}$$

which are equivalent to TRS in Eq. (2) and PHS in Eq. (3), respectively. Since $w(\boldsymbol{k}_\parallel)$ is a real integer number, we finally obtain the important relation

$$w(\boldsymbol{k}_\parallel) = \eta \, w(-\boldsymbol{k}_\parallel). \tag{18}$$

From Eq. (18), we find that the winding number for classes DIII and CI (i.e., $\eta = -1$) is an odd function of $\boldsymbol{k}_\parallel$. Therefore, the index $\mathcal{N}_{\mathrm{ZES}}$ in Eq. (9) becomes identically zero. This implies the absence of zero-energy states at the dirty surfaces

of DIII and CI nodal superconductors. On the other hand, the winding number for classes BDI and CII (i.e., $\eta = +1$) is an even function of $\boldsymbol{k}_\parallel$. Therefore, $\mathcal{N}_{\mathrm{ZES}} \neq 0$ is possible in these symmetry classes, which means that degenerate zero-energy states exist at the dirty surface. We summarize the results in Table I. At a clean surface, flat-band ZESs are expected irrespective of the symmetry classes of a nodal superconductor (see the fifth column of Table I). However, at a realistic dirty surface, the presence or absence of the flat-band ZESs depends on the symmetry class of the superconductor (see the sixth column of Table I). Namely, only the BDI or CII nodal superconductor has the potential to host degenerate ZESs at its dirty surface. This is the main conclusion of this paper.

The BdG Hamiltonian in class CI describes a spin-singlet superconductor [4]. Therefore, the flat-band ZESs of a spin-

singlet d_{xy}-wave superconductor are fragile against potential disorder [42,43]. Although several noncentrosymmetric superconductors have flat-band ZESs at their clean surface [12–16], the potential disorder completely lifts the degeneracy at zero energy [44,45] because the noncentrosymmetric superconductors belong to class DIII. The BdG Hamiltonian of a spin-triplet superconductor preserving spin-rotation symmetry belongs to class BDI [45]. Actually, the flat-band ZESs of the spin-triplet p_x-wave superconductor can retain their high degree of degeneracy even in the presence of the potential disorder [27,33,45]. In the following section, we investigate other examples of nodal superconductors that host robust flat-band ZESs under potential disorder. Unfortunately, we cannot find a specific model of a nodal superconductor in class CII. Even so, we demonstrate two practical models of topologically nontrivial nodal superconductors belonging to class BDI.

III. NODAL SUPERCONDUCTORS WITH THE NONZERO TOPOLOGICAL INDEX

A. BdG Hamiltonian in the single-band model

In this paper, we restrict our discussion to single-band superconductors belonging to class BDI. The BdG Hamiltonian in the single-band model is generally given by

$$\check{H}(\boldsymbol{k}) = \begin{bmatrix} \hat{h}(\boldsymbol{k}) & \hat{\Delta}(\boldsymbol{k}) \\ -\hat{\Delta}^*(-\boldsymbol{k}) & -\hat{h}^*(-\boldsymbol{k}) \end{bmatrix}, \tag{19}$$

$$\hat{h}(\boldsymbol{k}) = \varepsilon(\boldsymbol{k})\sigma_0 + \boldsymbol{g}(\boldsymbol{k}) \cdot \boldsymbol{\sigma} + \boldsymbol{V} \cdot \boldsymbol{\sigma}, \tag{20}$$

$$\hat{\Delta}(\boldsymbol{k}) = [\psi(\boldsymbol{k}) + \boldsymbol{d}(\boldsymbol{k}) \cdot \boldsymbol{\sigma}](i\sigma_2), \tag{21}$$

$$\varepsilon(\boldsymbol{k}) = \frac{\hbar^2 \boldsymbol{k}^2}{2m} - \mu_{\mathrm{F}}, \tag{22}$$

where σ_0 is the 2×2 unit matrix, m denotes the effective mass of an electron, and μ_{F} is the chemical potential. The spin-orbit-coupling potential is given by $\boldsymbol{g}(\boldsymbol{k}) = -\boldsymbol{g}(-\boldsymbol{k})$. The Zeeman potential induced by an external magnetic field is denoted by $\boldsymbol{V}$. The pair potential of a spin-singlet even-parity pairing order and that of a spin-triplet odd-parity pairing order are represented by $\psi(\boldsymbol{k}) = \psi(-\boldsymbol{k})$ and $\boldsymbol{d}(\boldsymbol{k}) = -\boldsymbol{d}(-\boldsymbol{k})$, respectively. In what follows, we assume the time-reversal invariant pairing orders which satisfy $\psi^*(\boldsymbol{k}) = \psi(\boldsymbol{k})$ and $\boldsymbol{d}^*(\boldsymbol{k}) = \boldsymbol{d}(\boldsymbol{k})$. The BdG Hamiltonian preserves PHS intrinsically as

$$\check{C}_+ \check{H}(\boldsymbol{k}) \check{C}_+^{-1} = -\check{H}(-\boldsymbol{k}), \quad \check{C}_+ = \begin{bmatrix} 0 & \sigma_0 \\ \sigma_0 & 0 \end{bmatrix}\mathcal{K}, \tag{23}$$

where $\check{C}_+^2 = +1$. For spinful fermionic systems, the TRS operator is generally defined by

$$\check{T}_- = \begin{bmatrix} i\sigma_2 & 0 \\ 0 & i\sigma_2 \end{bmatrix}\mathcal{K}, \tag{24}$$

obeying $\check{T}_-^2 = -1$. In the absence of the Zeeman potential (i.e., $\boldsymbol{V} = 0$), the BdG Hamiltonian $\check{H}(\boldsymbol{k})$ satisfies $\check{T}_- \check{H}(\boldsymbol{k}) \check{T}_-^{-1} = \check{H}(-\boldsymbol{k})$, which represents TRS of the BdG Hamiltonian. On the basis of the results in Sec. II, however, the index $\mathcal{N}_{\mathrm{ZES}}$ defined by using the chiral symmetry operator $\check{S}' = -i\check{T}_-\check{C}_+$ becomes identically zero. Alternatively, we assume that the

BdG Hamiltonian $\check{H}(\boldsymbol{k})$ satisfies

$$\check{T}_+ \check{H}(\boldsymbol{k}) \check{T}_+^{-1} = \check{H}(-\boldsymbol{k}), \tag{25}$$

where $\check{T}_+$ is a 4×4 antiunitary operator satisfying $\check{T}_+^2 = +1$. In the single-band model, the antiunitary operator $\check{T}_+$ is defined by combining the original TRS operator $\check{T}_-$ and a unitary operator $\check{R}$ as

$$\check{T}_+ = \check{R}\,\check{T}_- = \begin{bmatrix} \hat{r}(i\sigma_2) & 0 \\ 0 & \hat{r}^*(i\sigma_2) \end{bmatrix}\mathcal{K}, \tag{26}$$

$$\check{T}_- = \begin{bmatrix} i\sigma_2 & 0 \\ 0 & i\sigma_2 \end{bmatrix}\mathcal{K}, \quad \check{R} = \begin{bmatrix} \hat{r} & 0 \\ 0 & \hat{r}^* \end{bmatrix}, \tag{27}$$

where $\hat{r}$ is a 2×2 unitary operator. To satisfy the condition $\check{T}_+^2 = +1$, the form of the unitary operator $\hat{r}$ is restricted as

$$\hat{r} = -ie^{i\gamma/2}\boldsymbol{n} \cdot \boldsymbol{\sigma}, \tag{28}$$

where γ is an arbitrary real number and $\boldsymbol{n}$ is a unit vector in an arbitrary direction in spin space (see also Appendix B). As shown in Appendix C, it is possible to choose $\boldsymbol{n}$ in the specific direction because all the BdG Hamiltonians satisfying Eq. (26) are always unitarily equivalent to one another. In this paper, therefore, we choose $\boldsymbol{n}$ to be in the third spin direction and consider

$$\check{T}_z \check{H}(\boldsymbol{k}) \check{T}_z^{-1} = \check{H}(-\boldsymbol{k}), \tag{29}$$

$$\check{T}_z = \check{R}_z\,\check{T}_- = \begin{bmatrix} -ie^{i\gamma/2}\sigma_1 & 0 \\ 0 & ie^{-i\gamma/2}\sigma_1 \end{bmatrix}\mathcal{K}, \tag{30}$$

$$\check{R}_z = \begin{bmatrix} \hat{r}_z & 0 \\ 0 & \hat{r}_z^* \end{bmatrix}, \quad \hat{r}_z = -ie^{i\gamma/2}\sigma_3 \tag{31}$$

in what follows.

In Eq. (29), the normal-state Hamiltonian $\hat{h}(\boldsymbol{k})$ and the pair potential $\hat{\Delta}(\boldsymbol{k})$ respectively obey the relations

$$\hat{T}_z \hat{h}(\boldsymbol{k}) \hat{T}_z^\dagger = \hat{h}(-\boldsymbol{k}), \tag{32}$$

$$\hat{T}_z \hat{\Delta}(\boldsymbol{k}) \hat{T}_z^{\mathrm{T}} = \hat{\Delta}(-\boldsymbol{k}), \tag{33}$$

where $\hat{T}_z = -ie^{i\gamma/2}\sigma_1\mathcal{K}$ and T means a transpose of a matrix. The normal-state Hamiltonian in Eq. (20) is transformed into

$$\hat{T}_z \hat{h}(\boldsymbol{k}) \hat{T}_z^\dagger = \varepsilon(\boldsymbol{k})\sigma_0 - g_3(\boldsymbol{k})\sigma_3 + \sum_{j=1,2} V_j\sigma_j + \sum_{j=1,2} g_j(\boldsymbol{k})\sigma_j - V_3\sigma_3. \tag{34}$$

To satisfy Eq. (32), the normal Hamiltonian should have the form

$$\hat{h}_{\mathrm{BDI}}(\boldsymbol{k}) = \varepsilon(\boldsymbol{k})\sigma_0 + g_3(\boldsymbol{k})\sigma_3 + \sum_{j=1,2} V_j\sigma_j. \tag{35}$$

The pair potential in Eq. (21) is transformed into

$$\hat{T}_z \hat{\Delta}(\boldsymbol{k}) \hat{T}_z^{\mathrm{T}} = e^{i\gamma}[\psi(\boldsymbol{k}) - d_3(\boldsymbol{k})\sigma_3](i\sigma_2) + e^{i\gamma}\sum_{j=1,2} d_j(\boldsymbol{k})\sigma_j(i\sigma_2). \tag{36}$$

There are two possible choices of $\hat{\Delta}(\boldsymbol{k})$ and γ to satisfy Eq. (33). The first choice is

$$\hat{\Delta}_1(\boldsymbol{k}) = [\psi(\boldsymbol{k}) + d_3(\boldsymbol{k})\sigma_3](i\sigma_2), \tag{37}$$

setting $e^{i\gamma} = +1$. The second one is

$$\hat{\Delta}_2(\boldsymbol{k}) = \sum_{j=1,2} d_j(\boldsymbol{k})\sigma_j(i\sigma_2), \tag{38}$$

setting $e^{i\gamma} = -1$. As a consequence, the BdG Hamiltonian belonging to class BDI can be represented as

$$\check{H}_{\text{BDI}}(\boldsymbol{k}) = \begin{bmatrix} \hat{h}_{\text{BDI}}(\boldsymbol{k}) & \hat{\Delta}_\lambda(\boldsymbol{k}) \\ -\hat{\Delta}_\lambda^*(-\boldsymbol{k}) & -\hat{h}_{\text{BDI}}^*(-\boldsymbol{k}) \end{bmatrix}, \tag{39}$$

$$\hat{h}_{\text{BDI}}(\boldsymbol{k}) = \varepsilon(\boldsymbol{k})\sigma_0 + g_3(\boldsymbol{k})\sigma_3 + \sum_{j=1,2} V_j\sigma_j, \tag{40}$$

$$\hat{\Delta}_1(\boldsymbol{k}) = [\psi(\boldsymbol{k}) + d_3(\boldsymbol{k})\sigma_3]i\sigma_2, \tag{41}$$

$$\hat{\Delta}_2(\boldsymbol{k}) = \sum_{j=1,2} d_j(\boldsymbol{k})\sigma_j i\sigma_2. \tag{42}$$

When we choose the pair potential $\hat{\Delta}_1(\boldsymbol{k})$, the corresponding TRS operator is given by

$$\check{T}_{+,1} = \check{\theta}_z \check{T}_- = \begin{bmatrix} -i\sigma_1 & 0 \\ 0 & i\sigma_1 \end{bmatrix}\mathcal{K}, \tag{43}$$

$$\check{\theta}_z = \begin{bmatrix} -i\sigma_3 & 0 \\ 0 & i\sigma_3 \end{bmatrix}, \tag{44}$$

where the unitary operator $\check{\theta}_z$ physically means the spin rotation around the z axis. When we choose the pair potential $\hat{\Delta}_2(\boldsymbol{k})$, on the other hand, the corresponding TRS operator becomes

$$\check{T}_{+,2} = \check{\chi}(\pi)\,\check{\theta}_z\,\check{T}_- = \begin{bmatrix} \sigma_1 & 0 \\ 0 & \sigma_1 \end{bmatrix}\mathcal{K}, \tag{45}$$

$$\check{\chi}(\pi) = \begin{bmatrix} e^{i\pi/2}\sigma_0 & 0 \\ 0 & e^{-i\pi/2}\sigma_0 \end{bmatrix}, \tag{46}$$

where $\check{\chi}(\pi)$ represents the gauge transformation by π. In the following sections, we discuss two realistic examples of nodal superconductors whose BdG Hamiltonians satisfy Eq. (39).

B. Dresselhaus [110] superconductor

The first example may be an artificial superconducting hybrid, where a semiconductor thin film with the strong Dresselhaus [110] spin-orbit coupling is fabricated on a metallic superconductor [19,20] as shown in Fig. 1. The semiconductor thin film is superconductive due to the proximity-effect-induced s-wave pair potential. We also apply an in-plane magnetic field which induces the Zeeman potential on the thin
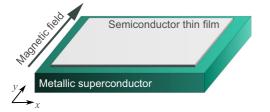

FIG. 1. Schematic image of a Dresselhaus [110] superconductor.
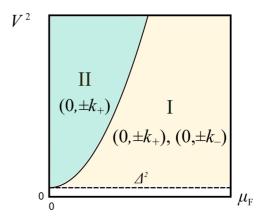

FIG. 2. Phase diagram of a Dresselhaus [110] superconductor. The solid line represents $V^2 = \mu_{\text{F}}^2$. The dashed line represents $V^2 = \Delta_s^2$.

film. Such a superconducting film is described by the BdG Hamiltonian

$$\check{H}_{\text{D}}(\boldsymbol{k}) = \begin{bmatrix} \hat{h}_{\text{D}}(\boldsymbol{k}) & \hat{\Delta}_{\text{D}}(\boldsymbol{k}) \\ -\hat{\Delta}_{\text{D}}^*(-\boldsymbol{k}) & -\hat{h}_{\text{D}}^*(-\boldsymbol{k}) \end{bmatrix}, \tag{47}$$

$$\hat{h}_{\text{D}}(\boldsymbol{k}) = \varepsilon(\boldsymbol{k})\sigma_0 + \beta k_x\sigma_3 + \sum_{j=1,2} V_j\sigma_j, \tag{48}$$

$$\hat{\Delta}_{\text{D}}(\boldsymbol{k}) = i\Delta_s\sigma_2, \tag{49}$$

where β is the strength of the Dresselhaus [110] spin-orbit coupling and Δ_s represents the amplitude of the proximity-induced s-wave pair potential. The BdG Hamiltonian in Eq. (47) satisfies

$$\check{T}_{+,1}\,\check{H}_{\text{D}}(\boldsymbol{k})\,\check{T}_{+,1}^{-1} = \check{H}_{\text{D}}(-\boldsymbol{k}), \tag{50}$$

$$\check{C}_+\,\check{H}_{\text{D}}(\boldsymbol{k})\,\check{C}_+^{-1} = -\check{H}_{\text{D}}(-\boldsymbol{k}), \tag{51}$$

with $\check{C}_+ = \tau_1\mathcal{K}$. The chiral symmetry operator of $\check{H}(\boldsymbol{k})$ is then given by

$$\check{S} = \check{T}_{+,1}\check{C}_+ = \begin{bmatrix} 0 & -i\sigma_1 \\ i\sigma_1 & 0 \end{bmatrix}. \tag{52}$$

The energy spectra of $\check{H}_{\text{D}}(\boldsymbol{k})$ are calculated to be

$$E(\boldsymbol{k}) = \pm\sqrt{\varepsilon^2(\boldsymbol{k}) + \beta^2 k_x^2 + V^2 + \Delta_s^2 \pm 2\eta(\boldsymbol{k})}, \tag{53}$$

$$\eta(\boldsymbol{k}) = \sqrt{\varepsilon^2(\boldsymbol{k})\beta^2 k_x^2 + V^2(\varepsilon^2(\boldsymbol{k}) + \Delta_s^2)}, \tag{54}$$

where $V = \sqrt{V_1^2 + V_2^2}$ represents the amplitude of the Zeeman field. A Dresselhaus [110] superconductor has two superconducting phases in terms of the number of point nodes on the Fermi surface: four point nodes in phase I and two point nodes in phase II. The phase diagram is shown in Fig. 2. Phase I is characterized by the relation $\Delta_s^2 < V^2 < \mu_{\text{F}}^2 + \Delta_s^2$. The nodal points are given by $(k_x,k_y) = (0,\pm k_+)$ and $(0,\pm k_-)$, with

$$k_{\pm} = \frac{\sqrt{2m(\mu_{\text{F}} \pm \sqrt{V^2 - \Delta_s^2})}}{\hbar}. \tag{55}$$

On the other hand, phase II is characterized by $V^2 > \mu_{\text{F}}^2 + \Delta_s^2$. The resulting nodal points are located at $(k_x,k_y) = (0,\pm k_+)$.

Now we focus on the flat-band ZESs appearing at the surface parallel to the y direction. The winding number in Eq. (5) can be further simplified to [8]

$$w(k_y) = -\frac{1}{2} \sum_{k_x \text{ at } m_1(\boldsymbol{k})=0} \text{sgn}[\partial_{k_x} m_1(\boldsymbol{k})]\text{sgn}[m_2(\boldsymbol{k})], \quad (56)$$

$$m_1(\boldsymbol{k}) = \varepsilon^2(\boldsymbol{k}) - \beta^2 k_x^2 - V^2 + \Delta_s^2, \quad (57)$$

$$m_2(\boldsymbol{k}) = 2\beta k_x. \quad (58)$$

The summation is carried out for wave numbers in the x direction k_x that satisfy $m_1(\boldsymbol{k}) = 0$ at a fixed k_y. The results for phase I are given by

$$w(k_y) = \begin{cases} -1 & \text{for } k_- < |k_y| < k_+, \\ 0 & \text{otherwise}, \end{cases} \quad (59)$$

and those for phase II are given by

$$w(k_y) = \begin{cases} -1 & \text{for } 0 \leqslant |k_y| < k_+, \\ 0 & \text{otherwise}. \end{cases} \quad (60)$$

The number of the zero-energy states at a dirty surface is evaluated by the index $\mathcal{N}_{\text{ZES}}$. By substituting Eqs. (59) and (60) into Eq. (9), we obtain

$$\mathcal{N}_{\text{ZES}} = \begin{cases} -\sum_{k_- < |k_y| < k_+} & \text{for phase I}, \\ -\sum_{0 \leqslant |k_y| < k_+} & \text{for phase II}. \end{cases} \quad (61)$$

When we treat the momentum k_y as a continuous variable, the discrete sum of k_y can be replaced with

$$\sum_{k_y} \rightarrow \frac{W}{2\pi} \int dk_y, \quad (62)$$

where W represents the length along the surface of the superconductor. By using Eq. (62), the index $\mathcal{N}_{\text{ZES}}$ in Eq. (61) is calculated to be

$$\mathcal{N}_{\text{ZES}} = \begin{cases} -[(W/\pi)(k_+ - k_-)]_{\text{G}} & \text{for phase I}, \\ -[(W/\pi)k_+]_{\text{G}} & \text{for phase II}, \end{cases} \quad (63)$$

where $[\cdots]_{\text{G}}$ is the Gauss symbol giving the integer part of the argument. The index $\mathcal{N}_{\text{ZES}}$ is nonzero in both phase I and phase II. Therefore, $|\mathcal{N}_{\text{ZES}}|$-fold-degenerate ZESs are expected at a dirty surface of the Dresselhaus [110] superconductor.

C. Helical p-wave superconductor with the in-plane magnetic field

The second example requires two-dimensional helical p-wave superconductivity. It is well known that a helical p-wave superconductor is fully gapped and hosts helical edge states at its surface reflecting a nonzero $\mathcal{Z}_2$ invariant. Here we apply an in-plane magnetic field [21,22]. The BdG Hamiltonian is described by

$$\check{H}_{\text{P}}(\boldsymbol{k}) = \begin{bmatrix} \hat{h}_{\text{P}}(\boldsymbol{k}) & \hat{\Delta}_{\text{P}}(\boldsymbol{k}) \\ -\hat{\Delta}_{\text{P}}^*(-\boldsymbol{k}) & -\hat{h}_{\text{P}}^*(-\boldsymbol{k}) \end{bmatrix}, \quad (64)$$

$$\hat{h}_{\text{P}}(\boldsymbol{k}) = \varepsilon(\boldsymbol{k})\sigma_0 + \sum_{j=1,2} V_j \sigma_j, \quad (65)$$

$$\hat{\Delta}_{\text{P}}(\boldsymbol{k}) = i\frac{\Delta_p}{k_{\text{F}}}[k_x \hat{\sigma}_1 + k_y \hat{\sigma}_2]\hat{\sigma}_2, \quad (66)$$
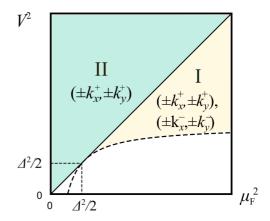

FIG. 3. Phase diagram of a helical p-wave superconductor under an in-plane Zeeman potential. The solid line represents $V^2 = \mu_{\text{F}}^2$. The dashed line represents $V^2 = -(\Delta_p^4/4\mu_{\text{F}}^2) + \Delta_p^2$.

where Δ_p is the amplitude of the helical p-wave pair potential and $k_{\text{F}} = \sqrt{2m\mu_{\text{F}}}/\hbar$ is the Fermi wave number. The Zeeman potential breaks TRS and spin-rotation symmetry simultaneously. Nevertheless, the BdG Hamiltonian is classified into class BDI [47,48], where

$$\check{T}_{+,2} \check{H}_{\text{P}}(\boldsymbol{k}) \check{T}_{+,2}^{-1} = \check{H}_{\text{P}}(-\boldsymbol{k}), \quad (67)$$

$$\check{C}_+ \check{H}_{\text{P}}(\boldsymbol{k}) \check{C}_+^{-1} = \check{H}_{\text{P}}(-\boldsymbol{k}) \quad (68)$$

are satisfied. The chiral symmetry operator is then given by

$$\check{S} = \check{T}_{+,2}\check{C}_+ = \begin{bmatrix} 0 & \sigma_1 \\ \sigma_1 & 0 \end{bmatrix}. \quad (69)$$

The energy eigenvalues of $\check{H}_{\text{P}}(\boldsymbol{k})$ are calculated to be

$$E(\boldsymbol{k}) = \pm\sqrt{\varepsilon^2(\boldsymbol{k}) + V^2 + \Delta_p^2 k^2 \pm 2\zeta(\boldsymbol{k})}, \quad (70)$$

$$\zeta(\boldsymbol{k}) = \sqrt{\varepsilon^2(\boldsymbol{k})V^2 + \Delta_p^2(V_1 k_x + V_2 k_y)^2}. \quad (71)$$

A helical p-wave superconductor under an in-plane magnetic field has three superconducting phases. Phase I appears when the parameters satisfy $-(\Delta_p^4/4\mu_{\text{F}}^2) + \Delta_p^2 < V^2 < \mu_{\text{F}}^2$ and $\mu_{\text{F}}^2 > \Delta_p^2/2$. The four nodal points on the Fermi surface are given by (k_x^+, k_y^+), $(-k_x^+, -k_y^+)$, (k_x^-, k_y^-), and $(-k_x^-, -k_y^-)$, with

$$k_x^{\pm} = k_0^{\pm} \cos(\theta_V), \quad k_y^{\pm} = k_0^{\pm} \sin(\theta_V), \quad (72)$$

$$k_0^{\pm} = \sqrt{k_{\text{F}}^2 - 2\kappa^2 \pm \sqrt{k_V^4 - 4\kappa^2(k_{\text{F}}^2 - \kappa^2)}}, \quad (73)$$

$$k_V = \frac{\sqrt{2mV}}{\hbar}, \quad \kappa = \frac{m\Delta_p}{\hbar^2 k_{\text{F}}}, \quad \theta_V = \arctan\left(\frac{V_2}{V_1}\right). \quad (74)$$

In phase II, appearing at $V^2 > \mu_{\text{F}}^2$, there are two nodal points at (k_x^+, k_y^+) and $(-k_x^+, -k_y^+)$. Finally, the superconducting states are topologically trivial in the rest of the parameter region. The phase diagram is shown in Fig. 3.

The winding number is calculated as

$$w(k_y) = -\frac{1}{2} \sum_{k_x \text{ at } m_1'(\boldsymbol{k})=0} \text{sgn}[\partial_{k_x} m_1'(\boldsymbol{k})] \text{sgn}[m_2'(\boldsymbol{k})], \quad (75)$$

$$m_1'(\boldsymbol{k}) = \varepsilon^2(\boldsymbol{k}) - V^2 + \Delta_p^2 \boldsymbol{k}^2, \quad (76)$$

$$m_2'(\boldsymbol{k}) = \Delta_p(V_1 k_y - V_2 k_x), \quad (77)$$

where the summation is carried out for k_x satisfying $m_1(\boldsymbol{k}) = 0$ at a fixed k_y. The results are given by

$$w(k_y) = \begin{cases} s_V & \text{for } |k_y^-| < |k_y| < |k_y^+|, \\ 0 & \text{otherwise} \end{cases} \quad (78)$$

for phase I and

$$w(k_y) = \begin{cases} s_V & \text{for } |k_y| < |k_y^+|, \\ 0 & \text{otherwise} \end{cases} \quad (79)$$

for phase II, with $s_V = \text{sgn}[\sin(\theta_V)]$. At $\theta_V = 0$ or π, the winding number becomes zero for all k_y because of $k_y^\pm = 0$. When θ_V is neither zero nor π, the winding number $w(k_y)$ can be either $+1$ or -1 depending on s_V. By substituting Eqs. (78) and (79) into Eq. (9), we obtain

$$\mathcal{N}_{\text{ZES}} = \begin{cases} s_V \sum_{|k_y^-| < |k_y| < |k_y^+|} & \text{for phase I,} \\ s_V \sum_{0 \leqslant |k_y| < |k_y^+|} & \text{for phase II.} \end{cases} \quad (80)$$

When we consider k_y as a continuous variable, the index $\mathcal{N}_{\text{ZES}}$ is calculated to be

$$\mathcal{N}_{\text{ZES}} = \begin{cases} s_V[(W/\pi)(|k_y^+| - |k_y^-|)]_G & \text{for phase I,} \\ s_V[(W/\pi)|k_y^+|]_G & \text{for phase II.} \end{cases} \quad (81)$$

The nonzero index $\mathcal{N}_{\text{ZES}}$ in Eqs. (80) and (81) suggests the existence of the stable $|\mathcal{N}_{\text{ZES}}|$-fold-degenerate ZESs at a dirty surface of a helical p-wave superconductor under an in-plane magnetic field.

IV. CONCLUSION

We studied the symmetry property of a nodal superconductor that hosts robust flat-band ZESs at its dirty surface. A nodal superconductor is topologically characterized by the winding number defined in a one-dimensional partial Brillouin zone. On the basis of the bulk boundary correspondence, we show the existence of flat-band ZESs at the clean surface of a nodal superconductor belonging to any of the symmetry classes BDI, CII, DIII, and CI. In the presence of potential disorder, we find that surface flat-band ZESs are robust only when the nodal superconductor belongs to either class BDI or class CII. In addition, we investigated two realistic examples of single-band nodal superconductors that belong to class BDI: a Dresselhaus [110] superconductor and a helical p-wave superconductor under a magnetic field. We found that flat-band ZESs are stable at a dirty surface in both cases. Therefore, such superconductors are promising candidates for observing the anomalous proximity effect, which is a drastic phenomenon caused by flat-band ZESs.

APPENDIX A: COMMUTATION RELATIONS OF SYMMETRY OPERATORS

We summarize the commutation relation among the symmetry operators. The Hamiltonian under consideration preserves time-reversal symmetry (TRS) and particle-hole symmetry (PHS) as

$$\mathcal{T} \mathcal{H}(\boldsymbol{k}) \mathcal{T}^{-1} = \mathcal{H}(-\boldsymbol{k}), \quad \mathcal{T}^2 = \eta_{\mathcal{T}}, \quad \eta_{\mathcal{T}} = \pm 1, \quad (A1)$$

$$\mathcal{C} \mathcal{H}(\boldsymbol{k}) \mathcal{C}^{-1} = -\mathcal{H}(-\boldsymbol{k}), \quad \mathcal{C}^2 = \eta_{\mathcal{C}}, \quad \eta_{\mathcal{C}} = \pm 1, \quad (A2)$$

where $\mathcal{T}$ and $\mathcal{C}$ are antiunitary operators. By combining TRS and PHS, the Hamiltonian also preserves chiral symmetry (CS) as

$$\mathcal{S} \mathcal{H}(\boldsymbol{k}) \mathcal{S}^{-1} = -\mathcal{H}(\boldsymbol{k}), \quad \mathcal{S} = e^{i\alpha_0} \mathcal{T} \mathcal{C}, \quad \mathcal{S}^2 = +1, \quad (A3)$$

where α_0 is determined so that $\mathcal{S}^2 = +1$ is satisfied. Since $\mathcal{T} \mathcal{C} \mathcal{C} \mathcal{T} = \eta_{\mathcal{T}} \eta_{\mathcal{C}}$, we immediately find $\mathcal{T} \mathcal{C} = \eta_{\mathcal{T}} \eta_{\mathcal{C}} \mathcal{T}^{-1} \mathcal{C}^{-1}$. This leads to the relation

$$(\mathcal{T}\mathcal{C})^2 = \eta_{\mathcal{T}} \eta_{\mathcal{C}} \mathcal{T} \mathcal{C} \mathcal{T}^{-1} \mathcal{C}^{-1}. \quad (A4)$$

From Eq. (A3), we also obtain

$$\mathcal{S}^2 = e^{2i\alpha_0}(\mathcal{T}\mathcal{C})^2 = +1. \quad (A5)$$

From Eqs. (A4) and (A5), we find the relation $\eta_{\mathcal{T}} \eta_{\mathcal{C}} \mathcal{T} \mathcal{C} \mathcal{T}^{-1} \mathcal{C}^{-1} = e^{-2i\alpha_0}$, which can be deformed as

$$\mathcal{C}\mathcal{T} = e^{2i\alpha_0} \eta_{\mathcal{T}} \eta_{\mathcal{C}} \mathcal{T} \mathcal{C}. \quad (A6)$$

By using Eq. (A6), we obtain

$$\begin{aligned} \mathcal{S}\mathcal{T} &= e^{i\alpha_0} \mathcal{T} \mathcal{C} \mathcal{T} = \mathcal{T} e^{-i\alpha_0} (e^{2i\alpha_0} \eta_{\mathcal{T}} \eta_{\mathcal{C}} \mathcal{T} \mathcal{C}) \\ &= \eta_{\mathcal{T}} \eta_{\mathcal{C}} \mathcal{T} \mathcal{S}, \end{aligned} \quad (A7)$$

$$\begin{aligned} \mathcal{S}\mathcal{C} &= e^{i\alpha_0} \mathcal{T} \mathcal{C} \mathcal{C} = e^{i\alpha_0} (e^{-2i\alpha_0} \eta_{\mathcal{T}} \eta_{\mathcal{C}} \mathcal{C} \mathcal{T}) \mathcal{C} \\ &= \eta_{\mathcal{T}} \eta_{\mathcal{C}} \mathcal{C} \mathcal{S}. \end{aligned} \quad (A8)$$

As a consequence, we find the commutation relation

$$[\mathcal{S}, \mathcal{T}] = [\mathcal{S}, \mathcal{C}] = 0 \quad (A9)$$

for $\eta_{\mathcal{T}} \eta_{\mathcal{C}} = +1$ and

$$\{\mathcal{S}, \mathcal{T}\} = \{\mathcal{S}, \mathcal{T}\} = 0 \quad (A10)$$

for $\eta_{\mathcal{T}} \eta_{\mathcal{C}} = -1$.

APPENDIX B: ANTIUNITARY OPERATOR $\check{T}_+$

We explain the expression of the antiunitary operator $\check{T}_+$ which satisfies $\check{T}_+^2 = +1$. By combining $\check{T}_-$ and an unitary

operator $\check{R}$, it is possible to define $\check{T}_+$ as

$$\check{T}_+ = \check{R}\,\check{T}_- = \begin{bmatrix} \hat{r}\,\hat{T}_- & 0 \\ 0 & \hat{r}^*\hat{T}_- \end{bmatrix}, \tag{B1}$$

$$\check{R} = \begin{bmatrix} \hat{r} & 0 \\ 0 & \hat{r}^* \end{bmatrix}, \quad \check{T}_- = \begin{bmatrix} \hat{T}_- & 0 \\ 0 & \hat{T}_- \end{bmatrix}, \quad \hat{T}_- = i\sigma_2\mathcal{K}, \tag{B2}$$

where $\hat{r}$ is a 2×2 unitary operator and $\check{T}_-^2 = -1$. The unitary operator $\hat{r}$ must satisfy

$$(\hat{r}\hat{T}_-)^2 = +1, \tag{B3}$$

so that the relation $\check{T}_+^2 = +1$ holds.

A general expression of a 2×2 unitary operator is given by

$$\hat{r} = e^{i\gamma/2}\hat{r}_0, \tag{B4}$$

$$\hat{r}_0 = \exp\left[-i\frac{\phi}{2}\boldsymbol{n}\cdot\boldsymbol{\sigma}\right] = \left[\cos\left(\frac{\phi}{2}\right)\sigma_0 - i\sin\left(\frac{\phi}{2}\right)\boldsymbol{n}\cdot\boldsymbol{\sigma}\right], \tag{B5}$$

where γ and ϕ are arbitrary real numbers and $\boldsymbol{n}$ is a unit vector in an arbitrary direction. By substituting Eq. (B4) into Eq. (B3), we obtain

$$\begin{aligned}(\hat{r}\,\hat{T}_-)^2 &= \hat{r}\,(i\sigma_2)\,\hat{r}^*\,(i\sigma_2) \\ &= -\hat{r}_0\,\sigma_2\,\hat{r}_0^*\,\sigma_2 \\ &= -\hat{r}_0^2 \\ &= -\left[\cos^2\left(\frac{\phi}{2}\right) - i\sin(\phi)\boldsymbol{n}\cdot\boldsymbol{\sigma} - \sin^2\left(\frac{\phi}{2}\right)\right] \\ &= +1. \end{aligned} \tag{B6}$$

Equation (B6) is satisfied only when $\phi = \pm\pi$. Therefore, the unitary operator $\hat{r}$ is restricted to

$$\hat{r} = -i\,e^{i\gamma/2}\boldsymbol{n}\cdot\boldsymbol{\sigma} \tag{B7}$$

to satisfy $\check{T}_+^2 = +1$.

APPENDIX C: UNITARY TRANSFORMATION

We consider the BdG Hamiltonian preserving time-reversal symmetry (TRS) as

$$\check{T}_+\,\check{H}(\boldsymbol{k})\,\check{T}_+^{-1} = \check{H}(-\boldsymbol{k}), \tag{C1}$$

$$\check{T}_+ = \begin{bmatrix} \hat{r}(i\sigma_2) & 0 \\ 0 & \hat{r}^*(i\sigma_2) \end{bmatrix}\mathcal{K}, \tag{C2}$$

where the 2×2 unitary operator $\hat{r}$ is given by

$$\hat{r} = -i e^{i\gamma/2}\boldsymbol{n}\cdot\boldsymbol{\sigma}, \tag{C3}$$

$$\boldsymbol{n} = (\cos\varphi\sin\theta, \sin\varphi\sin\theta, \cos\theta). \tag{C4}$$

When we apply a unitary transformation as

$$\check{H}_z(\boldsymbol{k}) = \check{U}\,\check{H}(\boldsymbol{k})\,\check{U}^\dagger, \quad \check{T}_z(\boldsymbol{k}) = \check{U}\,\check{T}_+\,\check{U}^\dagger, \tag{C5}$$

with

$$\check{U} = \begin{bmatrix} \hat{u} & 0 \\ 0 & \hat{u}^* \end{bmatrix}, \tag{C6}$$

$$\hat{u} = \begin{bmatrix} e^{i\varphi/2}\cos\left(\frac{\theta}{2}\right) & e^{-i\varphi/2}\sin\left(\frac{\theta}{2}\right) \\ -e^{i\varphi/2}\sin\left(\frac{\theta}{2}\right) & e^{-i\varphi/2}\cos\left(\frac{\theta}{2}\right) \end{bmatrix}, \tag{C7}$$

TRS of $\check{H}_z(\boldsymbol{k})$ is represented by

$$\check{T}_z\,\check{H}_z(\boldsymbol{k})\,\check{T}_z^{-1} = \check{H}_z(-\boldsymbol{k}), \tag{C8}$$

$$\check{T}_z = \check{R}_z\,\check{T}_- = \begin{bmatrix} -i e^{i\gamma/2}\sigma_1 & 0 \\ 0 & i e^{-i\gamma/2}\sigma_1 \end{bmatrix}\mathcal{K}, \tag{C9}$$

$$\check{R}_z = \begin{bmatrix} \hat{r}_z & 0 \\ 0 & \hat{r}_z^* \end{bmatrix}, \quad \hat{r}_z = -i e^{i\gamma/2}\sigma_3. \tag{C10}$$

The results suggest that a BdG Hamiltonian preserving TRS in Eq. (C1) is always unitarily equivalent to another BdG Hamiltonian preserving TRS in Eq. (C8).

[1] M. Z. Hasan and C. L. Kane, Rev. Mod. Phys. **82**, 3045 (2010).

[2] X.-L. Qi and S. C. Zhang, Rev. Mod. Phys. **83**, 1057 (2011).

[3] M. Sato and Y. Ando, Rep. Prog. Phys. **80**, 076501 (2017).

[4] A. P. Schnyder, S. Ryu, A. Furusaki, and A. W. W. Ludwig, Phys. Rev. B **78**, 195125 (2008).

[5] G. E. Volovik, *The Universe in a Helium Droplet* (Oxford University Press, New York, 2003).

[6] Y. Tanaka and S. Kashiwaya, Phys. Rev. Lett. **74**, 3451 (1995).

[7] Y. Asano, Y. Tanaka, and S. Kashiwaya, Phys. Rev. B **69**, 134501 (2004).

[8] M. Sato, Y. Tanaka, K. Yada, and T. Yokoyama, Phys. Rev. B **83**, 224511 (2011).

[9] A. P. Schnyder and P. M. R. Brydon, J. Phys.: Condens. Matter **27**, 243201 (2015).

[10] L. J. Buchholtz and G. Zwicknagl, Phys. Rev. B **23**, 5788 (1981).

[11] C. R. Hu, Phys. Rev. Lett. **72**, 1526 (1994).

[12] Y. Tanaka, Y. Mizuno, T. Yokoyama, K. Yada, and M. Sato, Phys. Rev. Lett. **105**, 097002 (2010).

[13] K. Yada, M. Sato, Y. Tanaka, and T. Yokoyama, Phys. Rev. B **83**, 064505 (2011).

[14] P. M. R. Brydon, A. P. Schnyder, and C. Timm, Phys. Rev. B **84**, 020501(R) (2011).

[15] A. P. Schnyder and S. Ryu, Phys. Rev. B **84**, 060504(R) (2011).

[16] A. P. Schnyder, P. M. R. Brydon, and C. Timm, Phys. Rev. B **85**, 024522 (2012).

[17] K. V. Samokhin and S. P. Mukherjee, Phys. Rev. B **94**, 104523 (2016).

[18] J. Alicea, Phys. Rev. B **81**, 125318 (2010).

[19] J. You, C. H. Oh, and V. Vedral, Phys. Rev. B **87**, 054501 (2013).

[20] S. Ikegaya, Y. Asano, and Y. Tanaka, Phys. Rev. B **91**, 174511 (2015).

[21] T. Mizushima, M. Sato, and K. Machida, Phys. Rev. Lett. **109**, 165301 (2012).

[22] C. L. M. Wong, J. Liu, K. T. Law, and P. A. Lee, Phys. Rev. B **88**, 060504(R) (2013).

[23] S. Deng, G. Ortiz, A. Poudel, and L. Viola, Phys. Rev. B **89**, 140507(R) (2014).

[24] A. Chen and M. Franz, Phys. Rev. B **93**, 201105(R) (2016).

[25] S. Kobayashi, K. Shiozaki, Y. Tanaka, and M. Sato, Phys. Rev. B **90**, 024516 (2014).

[26] S. Kobayashi, Y. Tanaka, and M. Sato, Phys. Rev. B **92**, 214514 (2015).

[27] Y. Tanaka and S. Kashiwaya, Phys. Rev. B **70**, 012507 (2004).

[28] Y. Asano, Y. Tanaka, A. A. Golubov, and S. Kashiwaya, Phys. Rev. Lett. **99**, 067005 (2007).

[29] S. Ikegaya, S.-I. Suzuki, Y. Tanaka, and Y. Asano, Phys. Rev. B **94**, 054512 (2016).

[30] Y. Tanaka and S. Kashiwaya, Phys. Rev. B **53**, R11957(R) (1996).

[31] Y. S. Barash, H. Burkhardt, and D. Rainer, Phys. Rev. Lett. **77**, 4070 (1996).

[32] H.-J. Kwon, K. Sengupta, and V. M. Yakovenko, Eur. Phys. J. B **37**, 349 (2004).

[33] Y. Asano, Y. Tanaka, and S. Kashiwaya, Phys. Rev. Lett. **96**, 097007 (2006).

[34] S. Ikegaya and Y. Asano, J. Phys.: Condens. Matter **28**, 375702 (2016).

[35] S. Higashitani, J. Phys. Soc. Jpn. **66**, 2556 (1997).

[36] H. Walter, W. Prusseit, R. Semerad, H. Kinder, W. Assmann, H. Huber, H. Burkhardt, D. Rainer, and J. A. Sauls, Phys. Rev. Lett. **80**, 3598 (1998).

[37] A. B. Vorontsov, Phys. Rev. Lett. **102**, 177001 (2009).

[38] S.-I. Suzuki and Y. Asano, Phys. Rev. B **89**, 184508 (2014).

[39] S.-I. Suzuki and Y. Asano, Phys. Rev. B **91**, 214510 (2015).

[40] M. Hakansson, T. Lofwander, and M. Fogelstrom, Nat. Phys. **11**, 755 (2015).

[41] S. Valentini, R. Fazio, V. Giovannetti, and F. Taddei, Phys. Rev. B **91**, 045430 (2015).

[42] Y. Asano, Phys. Rev. B **63**, 052512 (2001).

[43] Y. Tanaka, Yu. V. Nazarov, and S. Kashiwaya, Phys. Rev. Lett. **90**, 167003 (2003).

[44] R. Queiroz and A. P. Schnyder, Phys. Rev. B **89**, 054501 (2014).

[45] S. Ikegaya and Y. Asano, Phys. Rev. B **95**, 214503 (2017).

[46] Y. Xiong, A. Yamakage, S. Kobayashi, M. Sato, and Y. Tanaka, Crystals **7**, 58 (2017).

[47] K. Shiozaki and M. Sato, Phys. Rev. B **90**, 165114 (2014).

[48] M. T. Mercaldo, M. Cuoco, and P. Kotetes, Phys. Rev. B **94**, 140503 (2016).